J Therm Anal Calorim (2009) 96:827–834
DOI 10.1007/s10973-009-0049-9

Thermal analysis of protein–metallic ion systems

Xiao Hu · David Kaplan · Peggy Cebe

NATAS2008 Conference

Abstract Advanced thermal analysis methods, such as temperature modulated DSC (differential scanning calorimetry) and quasi-isothermal TMDSC were used to analyze the protein–metallic ion interactions in silk fibroin proteins. The precise heat capacities were measured and theoretically predicted in this study. To remove bound water and simplify the system, a thermal cycling treatment through both standard DSC and TMDSC was used to detect the underlying heat capacity and reveal the phase transitions of the silk–metallic salts system. Results show that K^+ metallic salts play the role of plasticizer in silk fibroin proteins, which reduces the glass transition (T_g) of the pure silk protein and negatively affects its structural thermal stability. On the other hand, Ca^{2+} metallic salts act as an anti-plasticizer, and increase the glass transition and the thermal stability of the silk protein structure. This indicates that the thermal analysis methods offer a new pathway to study protein–metallic ion systems, yielding very fruitful information for the study of protein structures in the future.

Keywords Anti-plasticizer · Beta pleated sheets crystal · *Bombyx mori* silk fibroin · Differential scanning calorimetry · Heat capacity · Metal ion

X. Hu · P. Cebe (✉)
Department of Physics and Astronomy, Tufts University, Medford, MA 02155, USA
e-mail: peggy.cebe@tufts.edu

X. Hu · D. Kaplan
Department of Biomedical Engineering, Tufts University, Medford, MA 02155, USA

Introduction

Proteins easily form bonds with a variety of metal ions, which provides many unique biological functions for the protein structures [1]. Many amino acid residues can serve as the potential ligands for a metallic cation [1], and therefore control the overall structural stability of proteins in different circumstance in vivo. The quarternary, tertiary, and secondary structures of the protein all could be affected by the interaction of metal ions [1]. Many approaches such as X-ray crystallography and nuclear magnetic resonance (NMR), have been previously used to study protein–metal ion interactions [2], providing precise information about the metal binding sites in the protein chains and determining the binding strength or the number of metal ions bound on protein molecules.

Advanced thermal analysis methods can also be used to investigate protein–metal ion systems. Metal ions may serve different functions when added to the protein creating a variety of structures, each having different thermal properties. A simple case is the behavior of metal ions as plasticizer or anti-plasticizer to the structure of protein. In this paper, we use silk fibroin protein as an example to discuss the protein–metal ion interactions through advanced thermal analysis methods.

Silk fibroin proteins are usually biosynthesized in specialized epithelial cells that are produced in the glands of silkworms [3, 4]. They have wide applications in the modern textile industry and the newly rising fields of biomedical science and engineering [5–8]. The domesticated silkworm protein (*B. mori* silk fibroin) consists of two protein sequences: the heavy chain (~350 kDa) and the light chain (~26 kDa), which are present with a 1:1 ratio and linked by a disulfide bond [3, 4]. The heavy chain sequence contains a large amount of highly repeating

(Gly-Ala-Gly-Ala-Gly-Ser)$_n$ amino acid domains [3, 4, 9, 10]. The production pathways in silk fiber formation are very complex but highly optimized. During the fiber spinning process from the silkworm gland, water soluble silk fibroin protein will rapidly transform to an insoluble fiber which contains a large amount of antiparallel beta-sheet crystals [3, 4, 9–12]. A combination of active dehydration, flow-induced forces, gradual acidification, and many metal ions such as K^+, Na^+, Ca^{2+}, Cu^{2+}, Mg^{2+}, are involved during the spinning process [3]. In a recent study [10], we have reported that a mesophase exists at the beginning stage of beta-sheet formation of silk fibroin proteins. With the help of the internal bound water molecules, a beta-sheet precursor structure is formed before the protein reaches its glass transition, which promotes the thermal crystallization of the beta-sheet structures above the glass transition temperature. The precise thermal analysis of silk protein with and without bound water has been reported in our previous work [10, 11, 13].

Beside the bound water molecules, metal ions also have been suggested to play a very important role in the unfolding and folding process of silk fibroin when it moves through the gland lumen and is spun out into air [3, 14–17]. Therefore, metal ions have attracted interest from both polymer and protein researchers. Many studies, performed during last decade [14–17], focused on the metallic ions effect on the silk fibroin solution. Among them, the effect of K^+ and Ca^{2+} ions has been found to be related to the unique functions in the silk fibroin proteins. Early studies by Magoshi et al. observed the concentration change of K^+ and Ca^{2+} metallic ions in the different divisions of the silkworm gland, and they pointed out that these ions can dramatically influence the conformation of silk fibers [14, 15]. In addition, Chen et al. reported that the content of major metallic ions changes within the secretory pathway of *B. mori* silkworm. It is found that the K^+ ions can break down the stable gel network of silk fibroin protein, while the Ca^{2+} tends to help the fibroin proteins maintain their stable network [16, 17]. These opposite functions for the K^+ and Ca^{2+} ions could be used to adjust the beta sheet crystal formation during the natural spinning process of silk fibers. Therefore, in this paper, we will focus on the thermal analysis of these two distinct metallic ions with silk fibroin, and discus their specific functions within the silk protein system.

Experimental section

Materials and preparation

The detailed silk fibroin preparation process has been reported previously [9–11]. Briefly, *Bombyx mori* silkworm cocoons (obtained from Tsukuba, Japan) were boiled in a 0.02 M Na_2CO_3 solution to extract the coated glue-like sericin protein [3]. The remaining silk fibroin was dissolved in a 9.3 M LiBr solution at 333 K (60 °C) for 4–6 h and then dialyzed with distilled water using a dialysis cassette for 2 days. After centrifugation and filtration to remove insoluble residues, the final 2 wt% silk fibroin aqueous solution was obtained.

The chloride salt powers containing metal ions, K^+ and Ca^{2+}, which are important for the biomacromolecular or protein functions, were purchased from Sigma Corp. with a purity of more than 99%. The salt powers (KCl and $CaCl_2$) were first dissolved in distilled water forming a 1.0 mass% ion salt aqueous solution. Then they were slowly mixed with the above silk fibroin aqueous solution using a pipette to avoid any possible protein aggregation during fast mixing in solution. The final solutions obtained for this study were based on a mass ratio of silk:KCl = 99:1 and silk:$CaCl_2$ = 98:2. These concentration ratios were chosen to mimic the strong interaction that silk has with the metal ions according to their physical condition within the silkworm gland [15, 16]. The homogenously mixed silk–ion salt solutions were then cast in polystyrene Petri dishes to make silk fibroin films with metal ions. The films were then put into a vacuum oven at room temperature for 5 days to remove moisture on their surfaces. Prior to any thermal procedure, the films were found to be generally non-crystalline and there was no strong signature of beta-pleated sheets crystal peak (around 1,625 cm^{-1}) in the FTIR absorption spectrum. A detailed spectrum verification method was reported in our previous work [9, 10].

Differential scanning calorimetry

The dried silk–KCl and silk–$CaCl_2$ samples (each about 5 mg) were encapsulated in Al pans and heated in a TA Instruments Q100 DSC, with purged dry nitrogen gas flow (50 mL/min), and equipped with a refrigerated cooling system. The instrument was calibrated with indium for heat flow and temperature. Standard mode DSC measurements were performed at a heating rate of 2 K/min. Temperature-modulated differential scanning calorimetry (TMDSC) measurements were also performed at a heating rate of 2 K/min with a modulation period of 60 s and temperature amplitude of 0.318 K.

Aluminum and sapphire reference standards were used for calibration of the heat capacity. The heat capacity measurement consisted of three runs, as described in our earlier work [9–11]. The first run is to use an empty Al reference pan versus an empty Al sample pan to obtain the baseline as background. The second run is to use an empty Al reference pan versus an Al sample pan with sapphire

standard to calibrate the calibration constant. The third run is to use an empty Al reference pan versus an Al sample pan with sample inside. The same empty Al reference pan needs to be used in all the runs and all the Al sample pans were prepared with same mass in order to maintain the same baseline. During the measurements, initial and final isotherms for all the three runs are used to assure that there had been no change in the instrument baseline in the time interval of these three measurements.

From a standard DSC measurement with a constant applied heating rate, the total heat capacity, which consists of both the reversing and non-reversing components, can be obtained from [9–13, 18–25]:

$$mC_p = K' HF/q \quad (1)$$

where K' is a calibration constant, HF is heat flow, q is the heating rate.

In TMDSC the "reversing heat capacity", which represent a reversed heat effect within the temperature range of the modulation, can be measured and calculated from [9–13, 18–25]:

$$\left| mC_p + C_s - C_r \pm \Delta C_{cell} \right| = (A_T/A)\left[(K/\omega)^2 + C_r^2\right]^{1/2} \quad (2a)$$

$$= K''(A_{HF})/A \quad (2b)$$

where C_p is the specific heat capacity of a sample with a mass m; C_s and C_r are the heat capacities of the sample pan and empty reference pan; ΔC_{cell} is the cell asymmetry correction which can be determined by running a series of empty pans with various mass differences [20]. On the right hand side of Eq. 2, A_T is the amplitude of temperature difference between sample and reference; A is the sample temperature modulation amplitude; K is Newton's law calibration constant; A_{HF} is the heat flow amplitude and K'' is a calibration constant at each individual temperature provided the same experimental conditions are maintained to assure the same heat transfer (e.g., same reference, same modulation frequency).

The quasi-isothermal TMDSC procedure was carried out over the temperature range of 403–512 K (130–239 °C) with a stepwise temperature increase of 3 K. The temperature modulation amplitude is 0.5 K, and the oscillation period is 1 min. Each quasi-isothermal run lasted 20 min per temperature step, and the data points collected during the last 10 min were averaged to calculated the heat capacity at a given temperature. The establishment of steady state was checked by plotting the Lissajous figures of modulated heat flow versus modulated temperature. A perfect ellipse needs to appear when steady state is reached, as occurred during the last 10 min of the quasi-isothermal step.

Results and discussion

Thermal cycling for bound water removal

In our previous studies, we have reported that bound water molecules inside silk fibroins can induce a low temperature glass transition during the heating process [10–13]. The first glass transition induced by silk–bound water system is essentially related to a mesophase which exists in the beginning stage, just before beta-sheet formation [10, 11]. It is also reported that the water content in the silk film will affect the temperature value of this water-induced glass transition [10, 11]. In the silk–metal ion films, we observed that bound water molecules also exist inside the films, even after 5 days of holding in a vacuum environment. The amount of bound water was around 3–5 mass%, measured by TG (Thermogravimetric Analysis) [11]. Although it is possible to observe and to discuss a complicated silk–ion–water system by thermal analysis, it is necessary to understand the simple ion effect on the silk fibroin protein first before attempting to model them in a complex system. Therefore, in the process of measuring the heat capacity of silk–metallic ion samples, we need to avoid the formation of this water-induced glass transition and to do so, it is necessary to remove the bound water molecules first. In our previous work [11], we developed a thermal cycling method to reduce the effect of the water-induced glass transition, which used a slow cyclic heating and cooling process ($\sim$2 K/min) to remove the bound water slowly, and avoid the silk protein–bound water glass transition (around 80 °C). In this way, finally the sample can reach a high temperature, above the water-induced glass transition, without displaying an obvious lower glass transition.

Figure 1a and b shows the standard DSC (total heat flow) of silk–KCl and silk–$CaCl_2$ samples, respectively, during the thermal cycling study. Figure 2a and b shows the corresponding TMDSC reversing heat flow traces of silk–KCl and silk–$CaCl_2$ samples using the same thermal cycling procedure. The thermal cycling method contains six cycles of a heat-cool-reheat process to monitor the change of heat flow during water removal at heating/cooling rates of $\pm$2 K/min. The four cycles take the film to steadily increasing temperatures, T_{end} (= 328, 358, 428, 528 K). For clarity, Figs. 1 and 2 only show the heating traces.

In the first heating process (curve 1, in Figs. 1, 2), silk–ion samples were heated from just below room temperature (288 K) to 328 K, and then they were cooled to 288 K. During this process, some intermolecular bound water molecules were evaporated resulting in a mass decrease in both silk–KCl and silk–$CaCl_2$ samples. Therefore, as the mass of the samples are reduced with the progressive evaporation of bound water, the staring point

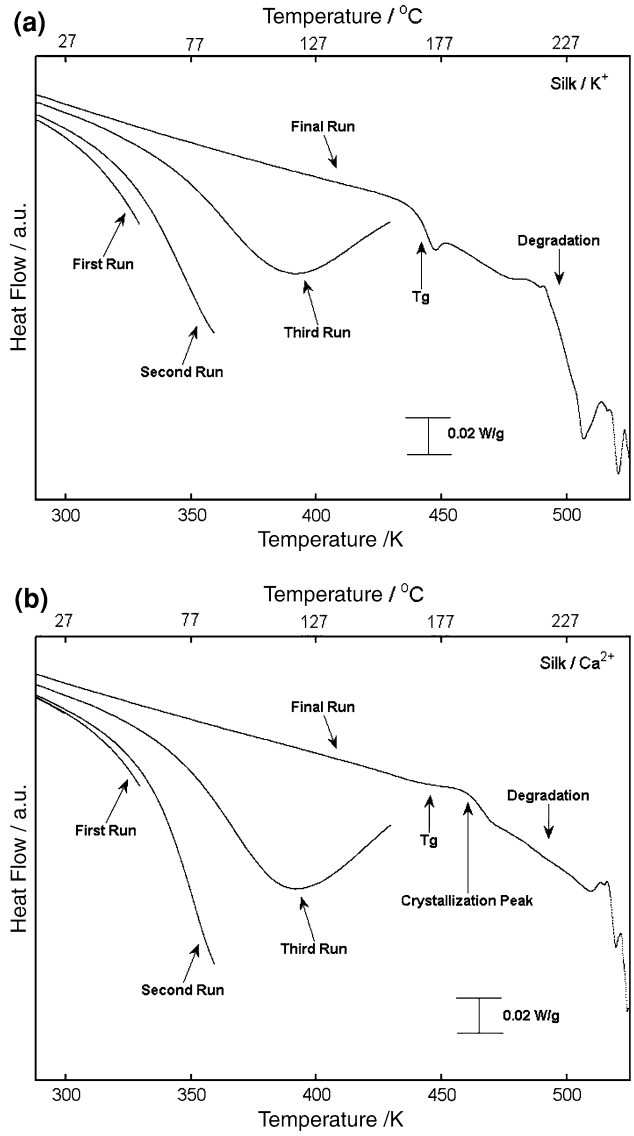

Fig. 1 Standard DSC total heat flow versus temperature for the **a** silk–KCl sample and **b** silk–$CaCl_2$ sample during a thermal cycling study. Four cycles (runs 1–4) of a heat-cool-reheat process were used to monitor the change of heat flow during bound water removal, at heating/cooling rates of ±2 K/min. Only the heating traces are shown for clarity. The final runs are the total heat flows of **a** silk–KCl sample and **b** silk–$CaCl_2$ sample without bound water. *Arrow* marks the temperatures such as the glass transition, crystallization peak, and the thermal degradation of silk–metallic salt systems

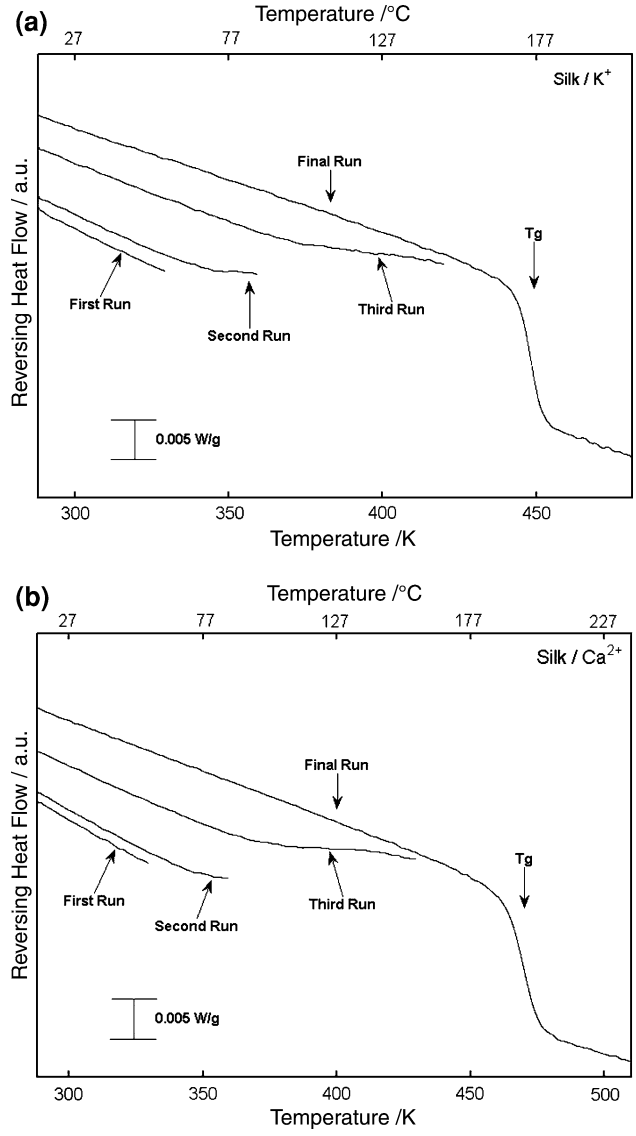

Fig. 2 TMDSC reversing heat flow versus temperature for the **a** silk–KCl sample and **b** silk–$CaCl_2$ sample during a thermal cycling study to remove bound water molecules. Four cycles (runs 1–4) were performed at heating/cooling rates of ±2 K/min with a modulation period of 60 s and temperature amplitude of 0.318 K. Only the heating traces are shown. The final runs are the reversing heat flows of **a** silk–KCl sample and **b** silk–$CaCl_2$ sample without bound water

of mass-normalized (mW/g) total heat flows and reversing heat flows in the second heating process are larger than the previous ones for both silk–KCl and silk–$CaCl_2$ samples, providing that no mass adjustment was performed during the measurements. This phenomenon occurred in each segment of the heating curves for both samples.

The total heat flows in Fig. 1a and b shows a curved trace of bound water lost through the four cycles, which presents as a endothermic process in the standard DSC heat flow traces. The reversing heat flow from TMDSC can avoid the non-reversing exothermal curve from water evaporation, and only the glass transition related reversing process can be seen in Fig. 2. In Fig. 2a and b, for both silk–KCl and silk–$CaCl_2$ samples, a straight line is the typical shape in the beginning part of reversing heat flow trace as temperature increase during each cycle. This indicates that the silk–ion–water system remains stable over this temperature region. In the end part of the reversing heat flow traces, the lines always shift up with the increase of temperature. This indicates the bound water molecules are slowly leaving the silk–ion–water system,

which make the mass of the measured system reduce gradually and results in an increasing heat flow trace. However, there is still no silk–water glass transition (heat flow shifting downward) occurring during the first through the third heating cycles. Finally, in the fourth run ($T_{end} = 528$ K), the total heat flow (Fig. 1) and the reversing heat flow (Fig. 2) show an almost straight curve without any bound water effect in the temperature region below 430 K, and reach the glass transition of the silk fibroin-metallic salts system without any bound water remaining inside. Therefore, the silk–ion system made through this cyclic procedure is free of water, and we can now measure the exact mass of the silk–KCl and silk–$CaCl_2$ samples at this time for calculating the precise specific heat capacity of silk–metallic salt systems.

In Fig. 1a and b, the final total heat flow traces of the silk–KCl and silk–$CaCl_2$ samples have many differences. The silk–KCl sample has a very clear glass transition curve but the non-isothermal crystallization peak of this system was absent, which may indicate that a slower cold crystallization process could be expected, compared to the pure silk fibroin we observed before [9, 10]. This is consistent with the argument of Chen et al. that the K^+ ions tend to break down the silk fibroin protein network for the beta-sheet crystal transition [16, 17]. The starting temperature of the silk–KCl degradation is around 490 K. In contrast, the silk–$CaCl_2$ sample has a clear non-isothermal crystallization peak after its glass transition region, and the starting degradation temperature of this system has moved up to around 512 K, which is also substantially higher than the starting degradation temperature of pure silk fibroin, which is around 498 K [9–11].

Heat capacity of silk fibroin–metallic salts system

The heat capacity of polymer and small molecules system has been well developed by Pyda [26–28] and has been used in our silk–water system [11, 13]. Briefly, the heat capacity of the mixed system of amorphous polymer and small molecules can be calculated from:

$$C_p(\text{poly}-\text{sm}) = C_{vib}(\text{poly}-\text{sm}) + C_{conf}(\text{poly}-\text{sm}) + C_{ext}(\text{poly}-\text{sm}) \quad (3)$$

where C_p(poly–sm) is the total heat capacity for the polymer-small molecules system, C_{vib}(poly–sm) is the vibrational heat capacity of this system, C_{ext}(poly–sm) represents the external heat capacity, and C_{conf}(poly–sm) stands for the conformational heat capacity. The major part of the total heat capacity is vibrational heat capacity (first term on the right side of (3)), which has been proved in silk fibroin to be almost equal to its total heat capacity [10, 11, 13]. Therefore, we can ignore the last two terms on the right in calculating the heat capacity for the protein-small molecule system. The vibrational heat capacities of the polymer-small molecules system in Eq. 3, can be estimated by the addition of the heat capacities of polymer, $C_{p,vib}$(poly), and small molecules, $C_{p,vib}$(sm), through the equation:

$$C_{vib}(\text{poly}-\text{sm}) = X_{poly} \cdot C_{p,vib}(\text{poly}) + X_{sm} \cdot C_{p,vib}(\text{sm}) \quad (4)$$

where X_{poly} and X_{sm} are the molar or mass fractions (depending on the units used for the heat capacities) of polymer and small molecules, respectively [26–28].

A theoretical model based on Eqs. 3 and 4 was then built for the solid and liquid heat capacity study of the protein–metallic salts system, which is:

$$C_p(\text{protein}-\text{salt})^{solid} = X_{protein} \cdot C_p(\text{protein})^{solid} + X_{salt} \cdot C_p(\text{salt}) \quad (5a)$$

$$C_p(\text{protein}-\text{salt})^{liquid} = X_{protein} \cdot C_p(\text{protein})^{liquid} + X_{salt} \cdot C_p(\text{salt}) \quad (5b)$$

and was used for the study the heat capacity of the silk protein–metallic salts system. In these expressions, protein substitutes for poly, and salt for sm in (3) and (4), and the heat capacities are understood to refer to the vibrational heat capacities.

The solid and liquid heat capacities of the pure silk fibroin has been measured previously [9–13] using differential scanning calorimetry (DSC), temperature-modulated DSC (TMDSC), and quasi-isothermal TMDSC. The best linear fit of the experimental data were found to be: $C_p(\text{silk})^{solid} = 0.134 + 3.696 \times 10^{-3}T$ [J g^{-1} K^{-1}] and $C_p(\text{silk})^{liquid} = 0.710 + 3.47 \times 10^{-3}T$ [J g^{-1} K^{-1}] over the temperature region from 200 to 450 K. Moreover, we developed a novel approach [13] to theoretically predict the heat capacity of silk protein by the sum of the heat capacities of its amino acid components. Results show it fit the experimental data well, and the calculated data are listed in Ref. 13. The heat capacities of the metallic salts have been measured many decades ago, and are listed partially (around room temperature) in most chemistry handbooks. For example, the heat capacity of potassium chloride in the low temperature region was measured by Nelson et al. in 1933 [29] and by Morrison et al. in 1957 [30] including the references inside; the heat capacity of calcium chloride was partially listed in a Calcium Chloride Handbook by Dynalene Inc. PA, USA [31].

Rather than use the literature values, we re-measured the heat capacity of the KCl and $CaCl_2$ samples to check for

experimental accuracy. The first several thermal cycles were performed to remove the possible water in the KCl and $CaCl_2$ samples. Then the "three run methods" was used to calculate the precise heat capacity of KCl and $CaCl_2$ in the temperature region of 250–600 K. The selected measured heat capacities of KCl and $CaCl_2$ are listed in Table 1 for reference. The data are very close to the previous literature reports [29, 30] and the chemistry handbooks [31]. Therefore, we used our measured data for the baseline calculation of the silk–metallic salt systems. It needs to be noted that, in most cases, the metallic salts without any bound water have a very high melting temperature (e.g., $T_m(KCl) = 1{,}048$ K and $T_m(CaCl_2) = 1{,}045$ K [29–32]), much higher than the degradation temperature of most proteins. Therefore, the metallic salt maintains itself in the same physical state throughout the temperature range of our study.

Figure 3 shows the specific heat capacity curve of silk protein–KCl (1.0 mass%) system from the TMDSC scan (solid curve) in the temperature region of the glass transition. The quasi-isothermal TMDSC traces are also shown for the comparison, using empty and filled circles. The quasi-isothermal heat capacity scans were measured from 403 to 512 K every 3 K to obtain the accurate solid and liquid state heat capacity values around the glass transition temperature region. In most of the temperature region of the solid state, the solid heat capacity obtained from these two methods matched each other very well, although a tiny slope shift was observed above 420 K. The two heat capacity traces in the liquid state at temperatures above the glass transition region are overlapped very well, no matter whether they are measured from reversing TMDSC or quasi-isothermal TMDSC.

The measured glass transition temperature of silk–KCl (1.0 mass%) from TMDSC trace is 171 °C (444 K), which is less than the T_g of pure silk fibroin proteins (178 °C). For comparison, the reversing specific heat capacity from a typical TMDSC heating scan of pure silk fibroin is plotted by the dashed curve. The solid and liquid state baselines of the pure silk protein are also shown (dashed lines) according to our previous discussion [10, 11]. Finally, the solid and liquid state heat capacity baselines of silk protein–KCl system (solid lines) were drawn according to Eqs. 5a and 5b. For the total solid specific heat capacity, $C_p(\text{protein-salt})^{solid}$, perfect agreement exists in the temperature region below T_g, indicating that only vibrational motions of silk and ion salt contribute to the heat capacity in this temperature region. For the total liquid specific heat capacity, C_p $(\text{protein–ion})^{liquid}$, good agreement also exists. Therefore, the only clear difference between the silk protein–KCl system and pure silk fibroin are the downshift of the glass transition. KCl plays a role of plasticizer in the silk protein structure and reduces the glass transition of the total system. However,

Table 1 Selected measured experimental heat capacities* of $CaCl_2$ and KCl in this study

Temperature (K)	Heat capacity of $CaCl_2$ (J g^{-1} K^{-1})	Heat capacity of KCl (J g^{-1} K^{-1})	Temperature (K)	Heat capacity of $CaCl_2$ (J g^{-1} K^{-1})	Heat capacity of KCl (J g^{-1} K^{-1})
250	0.640^{2}	0.672^{3}	420	0.729^{3}	0.755^{9}
260	0.642^{4}	0.674^{2}	430	0.734^{5}	0.758^{0}
270	0.646^{0}	0.678^{3}	440	0.741^{2}	0.765^{5}
273.15	0.652^{6}	0.678^{5}	450	0.753^{7}	0.772^{1}
280	0.654^{9}	0.683^{7}	460	0.755^{0}	0.777^{3}
290	0.664^{2}	0.691^{2}	470	0.758^{1}	0.785^{5}
298.15	0.669^{9}	0.697^{5}	480	0.761^{8}	0.793^{0}
300	0.670^{2}	0.699^{2}	490	0.764^{6}	0.800^{6}
310	0.676^{3}	0.703^{8}	500	0.767^{3}	0.808^{6}
320	0.681^{4}	0.709^{1}	510	0.775^{9}	0.814^{4}
330	0.685^{1}	0.712^{1}	520	0.784^{2}	0.823^{3}
340	0.689^{9}	0.714^{1}	530	0.787^{5}	0.831^{3}
350	0.693^{5}	0.719^{3}	540	0.794^{5}	0.838^{9}
360	0.700^{0}	0.724^{0}	550	0.798^{7}	0.847^{8}
370	0.703^{0}	0.72^{9}	560	0.803^{5}	0.854^{0}
380	0.705^{3}	0.733^{6}	570	0.806^{3}	0.857^{3}
390	0.712^{1}	0.738^{1}	580	0.810^{9}	0.864^{1}
400	0.718^{9}	0.744^{2}	590	0.816^{7}	0.873^{1}
410	0.724^{1}	0.748^{6}	600	0.826^{0}	0.880^{6}

* The fourth digit on the heat capacity data, shown using superscript, is not significant, but is included to show the range of values

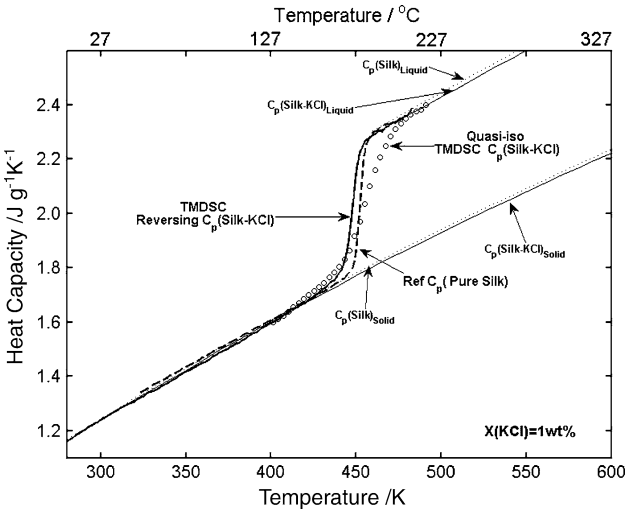

Fig. 3 Specific heat capacity curve of silk–KCl (1.0 wt%) system from the TMDSC scan (*solid curve*) and the quasi-isothermal TMDSC trace (*empty* and *filled circles*) in a temperature region of the glass transition. For comparison, specific heat capacity of pure silk fibroin is plotted in *dash line* with its solid and liquid state baselines (*dash lines*). The solid and liquid state heat capacity baselines of silk protein–KCl system (*solid line*) were drawn according to Eqs. 5a and 5b

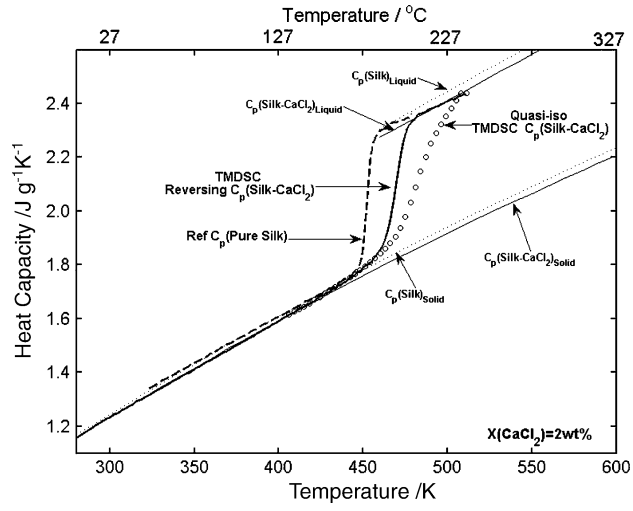

Fig. 4 Specific heat capacity curve of silk–$CaCl_2$ (2 wt%) system from the TMDSC scan (*solid curve*) and the quasi-isothermal TMDSC trace (*empty* and *filled circles*) in a temperature region of the glass transition. For comparison, specific heat capacity of pure silk fibroin is plotted with its solid and liquid state baselines (*dash lines*). The solid and liquid state heat capacity baselines of silk protein–$CaCl_2$ system (*solid line*) were drawn according to Eqs. 5a and 5b

not all metal ions have the same effect to the silk protein system, as we show below.

Figure 4 shows the specific heat capacity curve of silk protein–$CaCl_2$ (2.0 mass%) system from the TMDSC scan (solid curve) in a temperature region of its glass transition. A quasi-isothermal TMDSC trace is also shown for this system as a comparison, using empty and filled circles. The heat capacity traces in the solid state (below the glass transition region) are overlapped very well. In the liquid state, the quasi-isothermal (QI) TMDSC trace has a sharper slope compared with the TMDSC scan, but they finally match together above 230 °C (503 K). Furthermore, the QI-TMDSC trace within the glass transition region is shifted to much higher than the TMDSC trace. This could suggest a structural change may have occurred during the long time annealing of silk–$CaCl_2$ sample. Advanced infrared spectrum analysis will be performed to understand this phenomenon in future work.

The solid and liquid state heat capacity baselines of silk protein–$CaCl_2$ system (solid line) were drawn according to Eqs. 5a and 5b. Also shown are the TMDSC heat capacities for pure silk fibroin (dashed curve), and the solid and liquid state baselines of the pure silk protein (dotted lines), the same as in Fig. 3. It is clear that the glass transition temperature of silk–$CaCl_2$ system increases above the T_g of pure silk fibroin protein to a much higher temperature of 197 °C (470 K). However, the fitting of the non-crystalline baseline indicates that there are no crystals formed in the silk proteins. This means the $CaCl_2$ plays the role of an anti-plasticizer in the silk protein structure and increases the glass transition of the total system. Compared with the effect of KCl salts, $CaCl_2$ could make the structure of silk protein dramatically change according to reports in the literature [14–17]. Advanced structure analysis and microscopy observation in the future studies will provide us more detailed explanation of the effects of these ions on the protein structures. For now we see that advanced methods of thermal analysis can serve as a special method to detect the impact of the metal ions on the thermal properties of proteins, and provide subsequent information for the protein–metal interaction studies.

Conclusions

In this study, we utilize advanced thermal analysis methods to study the protein–metallic ion (salt) system. Silk fibroin proteins mixed with two different metallic ions (salts), silk–KCl and silk–$CaCl_2$ systems, were for the first time investigate by these methods, and their precise heat capacities were measured and theoretically predicted by TMDSC and Quasi-isothermal TMDSC in this study. To remove the bound water and simplify the system, a thermal cycling treatment through both standard DSC and TMDSC was used to detect the real heat capacity and solid to liquid phase transitions of the silk–metallic salts system. Results show that K^+ metallic salts play the role of plasticizer in silk fibroin proteins, which reduces the glass transition of the pure silk protein and negatively affects its structural

thermal stability. On the other hand, Ca^{2+} metallic salts act as an anti-plasticizer, and increase the glass transition and the thermal stability of the silk protein structure. This observation is consistent with the previous studies of silk–metallic interaction reported by other groups using different methods [14–17]. This indicates that advanced thermal analysis methods offer a new pathway to study protein–metallic ion systems, providing very fruitful information for the biomacromolecular researchers, which could be applied also in other protein structure studies.

Acknowledgements The authors thank the National Science Foundation Division of Materials Research, Polymers Program, for support of this research through grant DMR-0402849 and the MRI Program under DMR-0520655 for thermal analysis instrumentation.

References

1. Branden C, Tooze J. Introduction to protein structure. 2nd ed. New York: Garland Publishing Inc; 1998.
2. Rose PI. Protein-metal ion binding site: determination with proton magnetic resonance spectroscopy. Science. 1971;171:573–4.
3. McGrath K, Kaplan D, editors. Protein-based materials. Boston: Birkhauser Press; 1996. p. 103–33.
4. Jin HJ, Kaplan DL. Mechanism of silk processing in insects and spiders. Nature. 2003;424:1057–61.
5. Wang XY, Hu X, Daley A, Rabotyagova O, Cebe P, Kaplan DL. Nanolayer biomaterial coatings of silk fibroin for controlled release. J Control Release. 2007;121:190–9.
6. Wang X, Wenk E, Hu X, Castro GR, Meinel L, Wang X, et al. Silk coatings on PLGA and alginate microspheres for protein delivery. Biomaterials. 2007;28:4161–9.
7. Foo CWP, Kaplan DL. Genetic engineering of fibrous proteins: spider dragline silk and collagen. Adv Drug Deliv Rev. 2002; 54:1131–43.
8. Chen H, Hu X, Cebe P. Thermal properties and phase transitions in blends of Nylon-6 with silk fibroin. J Therm Anal Calorim. 2008;93:201–6.
9. Hu X, Kaplan D, Cebe P. Determining beta-sheet crystallinity in fibrous proteins by thermal analysis and infrared spectroscopy. Macromolecules. 2006;39:6161–70.
10. Hu X, Kaplan D, Cebe P. Dynamic protein-water relationships during beta-sheet formation. Macromolecules. 2008;41:3939–48.
11. Hu X, Kaplan D, Cebe P. Effect of water on the thermal properties of silk fibroin. Thermochim Acta. 2007;461:137–44.
12. Hu X, Lu Q, Kaplan DL, Cebe P. Microphase separation controlled beta-sheet crystallization kinetics in fibrous proteins. Macromolecules. 2009;42:2079–87.
13. Pyda M, Hu X, Cebe P. Heat capacity of silk fibroin based on the vibrational motion of poly(amino acid)s in the presence and absence of water. Macromolecules. 2008;41:4786–93.
14. Magoshi J, Magoshi Y, Nakamura S. In Kaplan D, Adams WW, Farmer B, Viney C, editors. Silk polymers. vol. 544. Washington, DC: American Chemical Society; 1994. p. 292.
15. Tsuda H, Kobayashi M, Tanaka T, Inoue S, Magoshi Y, Magoshi J. Different behavior of elution profile of silk fibroin on existence of calcium ion and potassium ion. Abstr Pap Am Chem Soc. 2002;223:POLY67.
16. Zhou L, Chen X, Shao ZZ, Huang YF, Knight DP. Effect of metallic ions on silk formation the mulberry silkworm, *Bombyx mori*. J Phys Chem B. 2005;109:16937–45.
17. Zhou L, Terry AE, Huang YF, Shao ZZ, Chen X. Metal element contents in silk gland and silk fiber of *Bombyx mori* silkworm. Acta Chim Sinica. 2005;63:1379–82.
18. Gaur U, Cao MY, Pan R, Wunderlich B. An addition scheme of heat-capacities of linear macromolecules – carbon backbone polymers. J Therm Anal Calorim. 1986;31:421–45.
19. Ishikiriyama K, Wunderlich B. Cell asymmetry correction for temperature modulated differential scanning calorimetry. J Therm Anal Calorim. 1997;50:337–46.
20. Xu H, Cebe P. Heat capacity study of isotactic polystyrene: dual reversible crystal melting and relaxation of rigid amorphous fraction. Macromolecules. 2004;37:2797–806.
21. Xu H, Cebe P. Heat capacity study of solution grown crystals of isotactic polystyrene. Macromolecules. 2005;38:770–9.
22. Wunderlich B, Jin YM, Boller A. Mathematical description of differential scanning calorimetry based on periodic temperature modulation. Thermochim Acta. 1994;238:277–93.
23. Wunderlich B. Macromolecular physics: crystal nucleation, growth, annealing, vol. 2. New York: Academic Press; 1976. p. 141.
24. Boller A, Okazaki I, Ishikiriyama K, Zhang G, Wunderlich B. Determination of cell asymmetry in temperature-modulated DSC. J Therm Anal Calorim. 1997;49:1081–108.
25. Pyda M, Boller A, Grebowicz J, Chuah H, Lebedev BV, Wunderlich B. Heat capacity of poly(trimethylene terephthalate). J Polym Sci Part B. 1998;36:2499–511.
26. Pyda M. Conformational contribution to the heat capacity of the starch and water system. J Polym Sci Part B. 2001;39:3038–54.
27. Pyda M. Conformational heat capacity of interacting systems of polymer and water. Macromolecules. 2002;35:4009–16.
28. Pyda M, Wunderlich B. Computation of heat capacities of liquid polymers. Macromolecules. 1999;32:2044–50.
29. Southard JC, Nelson RA. Low temperature specific heats. IV. The heat capacities of potassium chloride, potassium nitrate and sodium nitrate. J Am Chem Soc. 1933;55:4865–9.
30. Berg WT, Morrison JA. The thermal properties of alkali halide crystals 1. The heat capacity of potassium chloride, potassium bromide, potassium iodide, and sodium iodide between 2.8 degrees K and 270 degrees K. Proc R Soc Lond A Math Phys Sci. 1957;242:467–77.
31. Dynalene Inc. PA, USA. Calcium Chloride Handbook. Available online at www.dow.com
32. Sigma-Aldrich Corp. (Life Science). Products Descriptions Handbook.